



**HAL**  
open science

# Comprehensive optical and electrical characterization and evaluation of organic light-emitting diodes for visible light communication

Zahra Nazari Chaleshtori, Andrew Burton, Stanislav Zvanovec, Zabih Ghassemlooy, Petr Chvojka

## ► To cite this version:

Zahra Nazari Chaleshtori, Andrew Burton, Stanislav Zvanovec, Zabih Ghassemlooy, Petr Chvojka. Comprehensive optical and electrical characterization and evaluation of organic light-emitting diodes for visible light communication. *Optical Engineering*, 2020, 59 (04), pp.1. 10.1117/1.OE.59.4.046106 . hal-03341212

**HAL Id: hal-03341212**

**<https://amu.hal.science/hal-03341212>**

Submitted on 10 Sep 2021

**HAL** is a multi-disciplinary open access archive for the deposit and dissemination of scientific research documents, whether they are published or not. The documents may come from teaching and research institutions in France or abroad, or from public or private research centers.

L'archive ouverte pluridisciplinaire **HAL**, est destinée au dépôt et à la diffusion de documents scientifiques de niveau recherche, publiés ou non, émanant des établissements d'enseignement et de recherche français ou étrangers, des laboratoires publics ou privés.

# Comprehensive Optical and Electrical Characterization and Evaluation of OLEDs for VLC

Zahra Nazari Chaleshtori,<sup>a</sup> Andrew Burton,<sup>b</sup> Stanislav Zvanovec,<sup>a</sup> Zabih Ghassemlooy,<sup>b</sup> and Petr Chvojka<sup>a</sup>

<sup>a</sup>Czech Technical University in Prague, Faculty of Electrical Engineering, Department of Electromagnetic Field, Technická 2, Prague, Czech Republic, 16627

<sup>b</sup>Northumbria University, Faculty of Engineering and Environment, Optical Communications Research Group, Northumberland Road, Newcastle-upon-Tyne, UK, NE1 8ST

**Abstract.** In recent years, we have seen an increased use of organic light emitting diodes (OLEDs) for illumination in indoor environments due to the softer light compared with the conventional inorganic LEDs. In addition, OLEDs have been reported in visible light communication (VLC) systems, specifically for applications with lower data rates such as information boards, camera communications and positioning. However, OLEDs need extensive electrical and optical characterization if they are going to be fully exploited in VLC. This paper investigates characteristics of a range of flexible and rigid OLEDs and compares them with inorganic LEDs. We show that, OLEDs have highly linear power-current characteristics, and compared with rigid OLEDs with beam patterns closely matching Lambertian profile, the flexible OLED's radiation pattern is wider than Lambertian. Based on the measured experimental data, a new expression for the OLED's beam pattern, which follows the 3-term Gaussian profile, is proposed. Moreover, we show that using larger size OLED in VLC links offers improved bit error rate performance over a wide tilting angle up to 80° and a transmission path length up to 60 cm.

**Keywords:** organic LEDs; radiation pattern; spectrum; visible light communications.

Author E-mail: [[fnazarzah](mailto:fnazarzah@fel.cvut.cz); [xzvanove](mailto:xzvanove@fel.cvut.cz); [petr.chvojka](mailto:petr.chvojka@fel.cvut.cz)] [@fel.cvut.cz](mailto:fnazarzah@northumbria.ac.uk), [[z.ghassemlooy](mailto:z.ghassemlooy@northumbria.ac.uk); [andrew2.burton](mailto:andrew2.burton@northumbria.ac.uk)] [@northumbria.ac.uk](mailto:fnazarzah@northumbria.ac.uk)

## 1 Introduction

Visible light communications (VLC) is seen as a viable complementary technology to the radio frequency (RF) wireless communications in mostly indoor environments to meet the growing demands for high-speed wireless data transmission [1, 2]. VLC has the advantages of high energy efficiency (i.e., a green technology), no RF electromagnetic interference, license-free, and has inherent security and privacy compared with the RF technologies [3]. In VLCs, both conventional gallium-based light emitting diodes (LEDs) and organic LEDs (OLEDs) as well as white laser diodes are being used as a light source [1, 4]. The gallium-based LED based VLC systems, which utilize blue light to excite yellowish phosphors to synthesize white light, have

37 been extensively investigated in the literature [1, 5]. Whereas the red, green and blue (RGB) and  
38 phosphor laser diodes (LDs) based VLC require higher thermal stability of the phosphor due to a  
39 much greater optical power density [6]. Compared with the phosphor-based LD, the RGB LD is  
40 safer to the human eye due to the low illumination level blue light component [7].

41 OLEDs have interesting features over conventional and mainstream solid-state lighting and  
42 flat panel displays such as energy efficiency (i.e., they are environmentally friendly), brightness  
43 with no need for backlight as in LCD, sunlight style color-temperature tenability, very high color  
44 rendering index, small total stack thickness of an OLED being between 100-500 nm [8] and  
45 flexibility (i.e., can be used fabricated on plastics substrates or used in wearable clothes) [8-11].  
46 In addition, OLEDs with large photoactive areas are being used as pixels in smartphones, TVs  
47 and wearable devices, which offers the potential of infrastructure-to-device (I2D) and device-to-  
48 device (D2D) communications [12]. The latter is performed by transmitting and receiving the  
49 information data via the smartphone's OLED-based display pixels [13, 14] and the built-in  
50 cameras [15, 16].

51 OLEDs work in a similar manner to LEDs and use organic carbon-based molecules to  
52 generate electron-hole pairs but have different characteristics. There are two different types of  
53 OLED based on (i) small organic molecules deposited on a glass; and (ii) polymer (i.e., large  
54 plastic molecules) to produce light [17, 18]. However, the modulation bandwidth  $B_{\text{mod}}$  of OLEDs  
55 is orders of magnitude smaller compared with inorganic LEDs (i.e., in the kHz range compared  
56 with MHz in inorganic LEDs). The bandwidth limitation is due to the carrier lifetime and the  
57 parasitic resistor-capacitor (RC) effects, thus limiting their use in medium- to high-speed data  
58 communications [19]. However, OLED properties (i.e.,  $B_{\text{mod}}$ ) have been improved by using new  
59 materials with higher charge mobility [20]. In addition, a number of advanced communications

60 and signaling schemes as well as optimum driver circuits have been proposed to increase the  
61 transmission data rate [21, 22]. Future OLED applications will be in (i) medium to large panels  
62 for use in public places such as airports, shopping centers, train and bus stations, etc., [23, 24];  
63 and (ii) flexible or flat panel display technology for use in wearable biomedical devices in  
64 hospitals [25], which provide visual display, data communications and indoor localization. The  
65 novel devices of nano-OLEDs and microfluidic OLEDs are promising opening up new  
66 applications [26]. However, very little works have been reported on the optical and electrical  
67 characterization of different types of standard OLEDs used for illumination, which are essential  
68 when these devices are used in VLC. In this paper, we first experimentally investigate optical  
69 and electrical characteristics in terms of the threshold voltage, bias current, linear dynamic range,  
70 optical spectrum, optical radiation patterns and output optical power-current-voltage ( $L-I-V$ ) of a  
71 number of rigid and flexible (or curved) OLEDs within the context of VLC systems.  
72 Additionally, the characterization of organic devices is mostly limited to  $L-I-V$  or the frequency  
73 response measurements. In this work, the focus also is on other features of OLEDs (particularly  
74 large area flexible and rigid devices) such as dynamic resistance, linearity and radiation patterns,  
75 which are important in VLC, and compared them with the conventional inorganic sources. Large  
76 OLED panels compared with tiny OLEDs have lower modulation bandwidth, thus supporting a  
77 reduce level of throughputs in VLC [21, 22]. Therefore, more research utilizing large OLEDs  
78 with much lower bandwidth needs to be done. A number of schemes, including multi-carrier and  
79 multi-level modulation schemes, have been proposed to increase the data throughput. Here, we  
80 demonstrate the use of large size OLEDs as a transmitter in VLC systems employing a multi-  
81 band carrier-less amplitude and phase ( $m$ -CAP) modulation, which offers similar spectrum  
82 efficiency as the orthogonal frequency division multiplexing (OFDM) but at much reduced

83 implementation complexity. Hence, we evaluate the system performance in terms of the  
84 measured bit error rate (BER).

85 The rest of the paper is organized as follows. In Section 2, the structure of a typical OLED is  
86 described. In Section 3, the characterization of OLEDs is given followed by the experimental  
87 investigation of OLED-based VLC link in Section 4, and finally, conclusions are drawn in  
88 Section 5.

## 89 2 The Structure of OLEDs

90 The principal material in an organic semiconductor is either carbon or nitrogen [27]. The organic  
91 materials can be long-chain polymers (i.e., PLEDs) or small organic molecules (i.e., SMOLEDs)  
92 in a crystalline phase [19, 27]. The organic devices are based on the thin-film technology (see  
93 Fig. 1), where the general structure consists of two or more organic semiconductor materials  
94 sandwiched between oppositely polarized electrodes. OLEDs have a low-pass filter transfer  
95 function with the cut-off frequency given by [28]:

$$96 \quad f_{3\text{-dB}} = \frac{1}{2\pi(\tau_s + \tau_c)}, \quad (1)$$

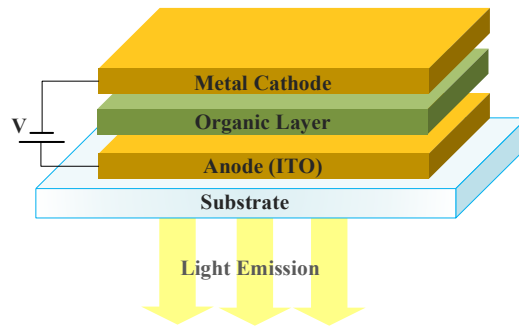
97 where  $\tau_s$  is the differential carrier lifetime, which is inversely proportional to the drive current  
98 [28].  $\tau_c \sim RC$ , where  $R$  is the effective resistance of the OLED and  $C$  is the plate capacitance,  
99 which is defined as [1]:

$$100 \quad C = \frac{A\epsilon_0\epsilon_r}{d}, \quad (2)$$

101 where  $A$  is the OLED photoactive area,  $d$  is the OLED thickness, and  $\epsilon_0$  and  $\epsilon_r$  are the  
102 permittivity of free space and relative dielectric constant of the organic layer, respectively.

103 Note that, as in LEDs,  $B_{\text{mod}}$  of OLEDs is inversely proportional to  $A$ , hence much lower  
104 bandwidth than small area gallium-based LEDs [4]. In addition, in highly bandlimited organic

105 VLC systems the inter-symbol interference (ISI) leads to the significant BER degradation. A  
106 number of schemes have been proposed to overcome both lower  $B_{\text{mod}}$  and the ISI including:  
107 high-level modulations [29, 30], equalization schemes such as the artificial neural network  
108 (ANN) [21, 22], specially designed receivers [31-35], single-input multiple-output (SIMO) or  
109 multiple-input multiple-output (MIMO) configuration [36, 37], bit/power loading [22, 38] and  
110 power pre-emphasis [30, 39].



111 **Fig. 1** The OLED structure.

111

### 112 **3 Characterization of OLEDs**

#### 113 *3.1 Experimental Test-bed*

114 To carry out comprehensive tests and measurements for characterization of the OLEDs, we have  
115 developed an experimental test-bed, as shown in Fig. 2. The test-bed includes an arbitrary  
116 function generator AFG Agilent 3252, driving circuits, OLEDs, optical receiver (ORx) Thorlabs  
117 PDA100A2 (consisting of a photodiode (PD) and a transimpedance amplifier (TIA)),  
118 spectrometer Thorlabs CCS200 with CCSB1 cosine corrector with a diameter of 8.5 mm and the  
119 digital LED lux meter DT-3809.

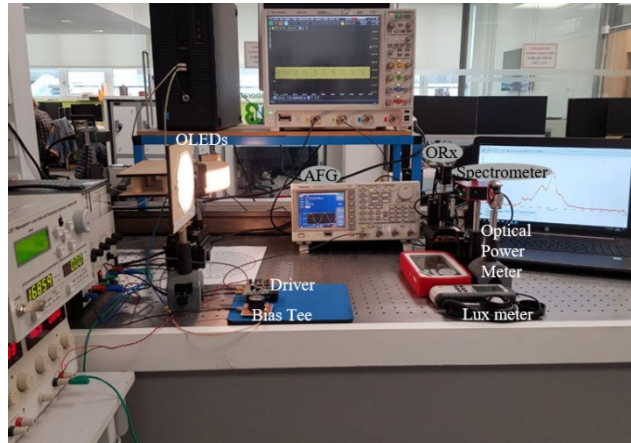
120 Five OLEDs - four different rigid OLEDs from LG (i.e., N6OA40C, N6SC40C, N6BA40C  
121 and N6SB40 denoted as  $D_1$  to  $D_4$ ) and a single flexible OLED from UNISAGA (denoted as  $D_5$ ),

122 see Fig. 3, were investigated in terms of their optical and electrical characteristics including the  
 123 optical spectrum,  $L-I-V$  curves, optical radiation pattern and  $B_{\text{mod}}$ . All experiments were carried  
 124 out under the same controlled environments (within a dark room) and for each set-up, five sets of  
 125 measurements were carried to ensure repeatability and correctness. The main parameters of  
 126 tested OLEDs are given in Table 1.

127 **Table 1** The OLEDs under test.

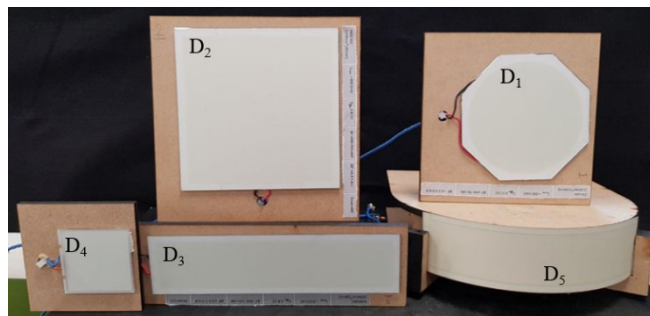
OLED	Size (mm)	Device thickness (mm)	Luminous efficiency (lm/W) (Bias current $I_B$ (mA))	Luminous flux (lm) ( $I_B$ (mA))
<b>Rigid</b>				
D <sub>1</sub> : N6OA40C	48.7 (Radius)	1	55 (230)	75 (230)
D <sub>2</sub> : N6SC40C	140 × 140	0.88	55 (480)	150 (480)
D <sub>3</sub> : N6BA40C	200 × 50	1.77	53 (230)	73 (230)
D <sub>4</sub> : N6SB40	55 × 53	1.97	55 (62)	20 (62)
<b>Flexible</b>				
D <sub>5</sub>	200 × 50	0.41	53 (230)	75 (230)

128



129

130 **Fig. 2** An experimental test-bed for characterization of OLEDs.



131

132 **Fig. 3** Different OLEDs (D<sub>1</sub> to D<sub>5</sub>) under test.

133 3.2 Optical and Electrical Characterization

134 3.2.1 OLED's spectrum

135 To measure the spectrum profiles of OLEDs, a spectrometer with a cosine corrector capturing  
136 light over a 180° angle was used. The measured normalized optical spectrum (averaged over five  
137 sets of measurements) for a range of  $I_B$  for  $D_1$  is depicted in Fig. 4(a) showing R, G and B  
138 components at the peak wavelengths of 613, 555 and 450 and 480 nm, respectively. OLEDs  $D_1$ -  
139  $D_5$  and an inorganic white LED (LUXEON cool white rebel star LED (5650K) sr-01) display  
140 broad-spectrum profiles with RGB components, see Fig. 4(b). For the flexible OLED, the R  
141 component is at a slightly higher wavelength of 620 nm, whereas B and G components have  
142 lower intensities compared with the rigid OLEDs. This is attributed to the lower conversion  
143 efficiency of B and G materials in  $D_5$ . Whereas, for the inorganic LED the dominant color is B.

144 Next, we investigate the spectrum (i.e., the color) of the  $D_1$  under different dimming levels  
145 (i.e.,  $10 \text{ mA} < I_B < 300 \text{ mA}$ ) as shown in Fig. 4(c). Note, the normalized intensity profiles are  
146 almost the same with low intensity variation of the peak intensities. Thus, indicating no  
147 significant changes in the color of OLEDs in contrast to the inorganic LEDs reported in [40].

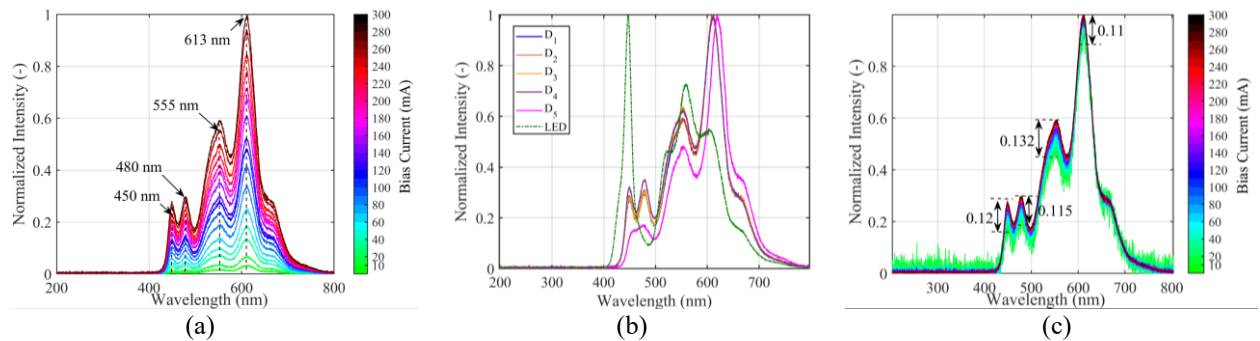


**Fig. 4** (a) The optical spectrum of  $D_1$  are normalized to the maximum  $I_B$  with peak wavelengths marked where

the legend color scale represents  $I_B$ , (b) all devices outputs and a gallium-based white LED at their

corresponding maximum  $I_B$ , and (c) the optical spectrum of  $D_1$  for a range of  $I_B$  where each of the spectral

responses were normalized to unity and then superimposed on top of each other.

148



149 3.2.2 OLED  $L$ - $I$ - $V$  curves

150 The  $I$ - $V$  curves of the OLED panels under test were measured using a source meter (Keithley  
 151 SourceMeter Series 2400) and their illuminance was measured using a lux meter, where the  
 152 distance between the OLED and the lux meter was fixed at  $15 \times$  the horizontal dimension of the  
 153 OLED (as recommended by lux meter manufacturer). The measured  $L$ - $I$ - $V$  curves of the OLEDs  
 154 are illustrated in Fig. 5 showing linear characteristics with sufficient dynamic ranges. Table 2  
 155 summarizes the measured maximum current  $I_{B\text{-Max}}$ , threshold voltage  $V_{\text{th}}$ , range of  $I_B$  in the linear  
 156 part  $\Delta I$ , range of voltage in the linear part  $\Delta V$  and slope of the  $V$ - $I$  curve (i.e., inverse of the  
 157 dynamic resistance for all OLEDs at  $I_B$ ). Note, with a wide linear range  $L$ - $I$  range around  $I_B$   
 158 higher signal levels can be used for intensity modulation of the OLED, thus higher signal to  
 159 noise ratio and lower BER). Using linear regression curve-fitting, the plots in Fig. 5 show a  
 160 highly linear  $L$ - $I$  relationship. To compare the linearity of inorganic LEDs with OLEDs we have  
 161 used root mean square error (RMSE) i.e.,  $RMSE = \sqrt{(\sum P_I - P_{\text{mod}})^2/n}$ , where  $P_I$  and  $P_{\text{mod}}$  are  
 162 the measured and linear modelled optical powers, respectively and  $n$  is the number of measured  
 163 samples, see Table 3. Note, OLEDs tested in this work show a considerably lower RMSE  
 164 compared with the inorganic LEDs (i.e., RGB, 5 mm RGB, RAGB (RGB + amber LEDENGIN  
 165 LZ4-00MA00) and a COBLED (LUSTREON 4W 48led COBLED Chip)).

166 **Table 2** The parameters of OLEDs under test

OLED	$I_{B\text{-Max}}$ (mA)	$V_{\text{th}}$ (V)	Slope ( $\Delta I/\Delta V$ )	Dynamic resistance ( $\Omega$ ) ( $I_B$ (mA))
D <sub>1</sub>	300	4.6	0.263	3.8 (160)
D <sub>2</sub>	800	4.8	0.400	2.5 (400)
D <sub>3</sub>	350	4.8	0.225	4.4 (160)
D <sub>4</sub>	100	5.0	0.083	12.0 (60)
D <sub>5</sub>	300	7.0	0.033	4.3 (180)

167

168

169

**Table 3** The parameter of linearity of inorganic LEDs and OLEDs

OLED	RMSE	Ga LED	RMSE		
			R	G	B
D <sub>1</sub>	$2 \times 10^{-14}$	RGB	0.004	0.07	0.008
D <sub>2</sub>	$3 \times 10^{-14}$	RAGB	0.0036	0.0025	0.0032
D <sub>3</sub>	$1.1 \times 10^{-14}$	5 mm RGB	0.0016	0.0027	0.0047
D <sub>4</sub>	$1.3 \times 10^{-7}$	COBLED		0.5114	
D <sub>5</sub>	$1.2 \times 10^{-14}$				

170

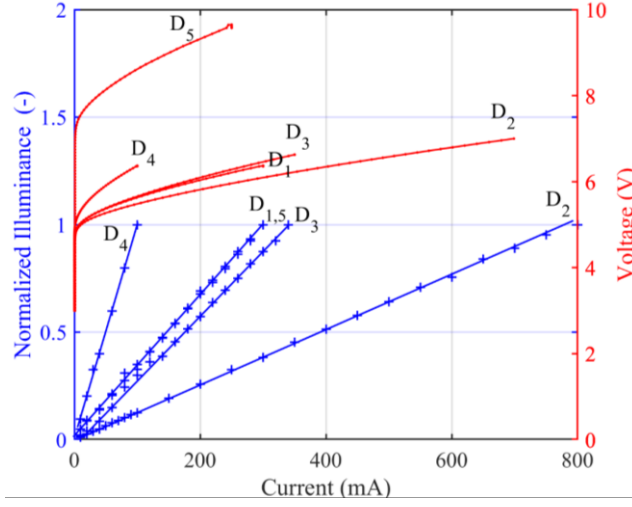


**Fig. 5** The  $L-I-V$  curves for OLEDs where  $V-I$  and  $L-I$  curves are associated to each device marked as D<sub>1</sub> to D<sub>5</sub>.

171

172 *3.2.3 Optical radiation pattern*

173 The optical radiation pattern describes the spatial intensity distribution of light emitted from the  
 174 OLEDs, which is important, especially when analyzing the coverage and signal distribution in  
 175 VLC links. The light intensity of LEDs defined in terms of the angle of irradiance  $\theta$  is given by  
 176 [1, 2]:

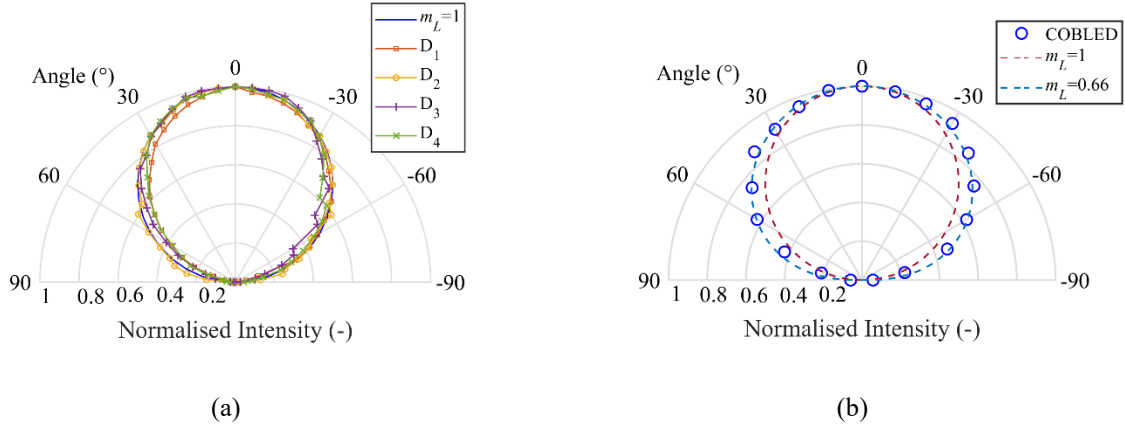
$$177 \quad I(\theta) = \frac{m_L + 1}{2\pi} I(0) \cos^{m_L}(\theta), \quad \theta = \left[-\frac{\pi}{2}, \frac{\pi}{2}\right] \quad (3)$$

178 where  $I(0)$  is the center luminous intensity of an LED and  $m_L$  is Lambertian order given as [1]:

$$179 \quad m_L = -\frac{\ln(2)}{\ln[\cos(\theta_{1/2})]}, \quad (4)$$

180 where  $\theta_{1/2}$  is the semi-angle at half illuminance.

181 In order to empirically derive the beam patterns of rigid OLEDs and determine Lambertian  
 182 order of emission, a lux meter was used to measure the luminance, as shown in Fig. 6(a). As  
 183 expected, the profiles are complete hemispheres close to Lambertian emitter with  $m_L = 1$  in  
 184 contrast to the intensity profile of a COBLED with  $m_L = 0.66$  as shown in Fig. 6(b).



185 **Fig. 6** The polar dimensional radiation patterns for: (a) rigid OLEDs for D<sub>1</sub>, D<sub>2</sub>, D<sub>3</sub>, and D<sub>4</sub> and (b) a COBLED.

186

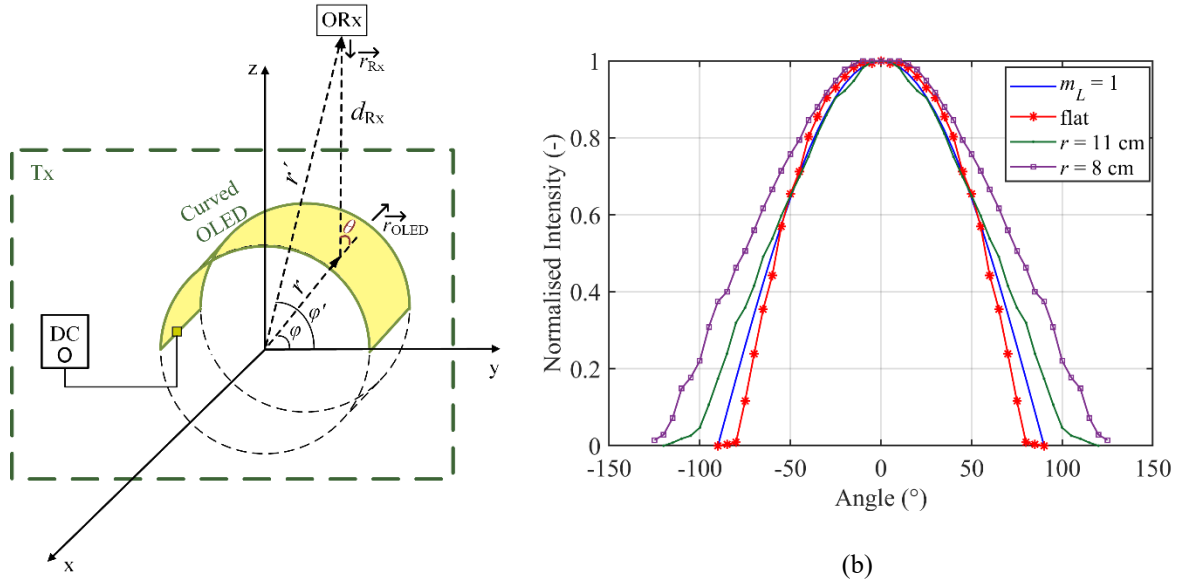
187 With reference to Fig. 7(a), the irradiance angle  $\theta$  is given as:

$$188 \quad \theta = \arccos \frac{\vec{d}_{Rx} \cdot \vec{r}_{OLED}}{\left| \vec{d}_{Rx} \right| \left| \vec{r}_{OLED} \right|}, \quad (5)$$

189 where  $\vec{r}_{OLED}$  and  $\vec{r}_{Rx}$  are the norm vectors of the OLED and the ORx, respectively, and  $d_{Rx}$  is a  
 190 distance of OLED and ORx. The position of OLED and the ORx can be considered as  $(r, \varphi, x_1)$   
 191 and  $(r', \varphi', x_2)$  in the cylindrical coordinate, respectively, where  $r$  is the OLED curvature radius,  
 192  $0 < \varphi < 180^\circ$  and  $x_1$  refers to the OLED's width. Thus, we have:

$$193 \quad \cos(\theta) = \frac{r' \cos \varphi' \cos \varphi - r \cos^2 \varphi + r' \sin \varphi' \sin \varphi - r \sin^2 \varphi}{r' - r}. \quad (6)$$

194 To investigate the intensity profiles of flexible OLED, the device was bent with the different  
 195 radius of curvatures  $r$  of 11 cm and 8 cm to have quadrature and half-circle light sources, as  
 196 shown in Fig. 7(a). The measured radiation pattern shows a symmetry about the origin  $0^\circ$  not  
 197 fitting Lambertian radiation pattern, see the solid blue line for  $m_L = 1$  in Fig. 7(b). Note, the  
 198 OLED with higher  $r$  displays a radiation beam profile closer to Lambertian with  $m_L = 1$ . The  
 199 radiation angle ranges for  $\theta_{1/2}$  for the flat 11 and 8 cm curved OLEDs are  $58^\circ$ ,  $65^\circ$ ,  $75^\circ$ ,  
 200 respectively.



201 **Fig. 7** (a) OLED panel bent in different curvature radius  $r$  of 11 and 8 cm and (b) two-dimensional intensity pattern.

202 A numerical fitting method was used to estimate the radiation pattern parameters of flexible  
 203 OLEDs. The 3-term Gaussian model provided the best fit to describe the radiation patterns of  
 204 OLEDs, which is given by:

$$205 \quad I(\theta) = \sum_{k=1}^q a_k \times \exp\left(-\left(\frac{\theta - b_k}{c_k}\right)^2\right), \quad (7)$$

206 where  $a_k$ ,  $b_k$ ,  $c_k$ , are parameters estimated by the curve fitting tool,  $k$  is the order and  $q$  is the term  
 207 of Gaussian model, which is considered to be 3 for the best match with the empirical data. The  
 208 RMSE analysis has been carried out on the modelled and measured intensity profiles to assess

209 the accuracy of the model. For the curved OLED, the RMSE values are 0.016 and 0.018 for  $r$  of  
 210 11 and 8 cm, respectively, which are less than the standard error limit of 0.05 [41]. The  
 211 numerical fitting parameters are shown in Table 4 for OLEDs with  $r$  of 11 and 8 cm. Note,  $a_k$  is  
 212 the peak of the  $k^{\text{th}}$  term of 3-term Gaussian (i.e.,  $a_1 \sim 1$ ), and  $b_k$  is the angular position of peak  
 213 referred to the each Gaussian as  $b_1 \sim 0$ .  $c_k$  is the standard deviation of the  $k^{\text{th}}$  term of the 3-term  
 214 Gaussian with higher values representing a wider profile.

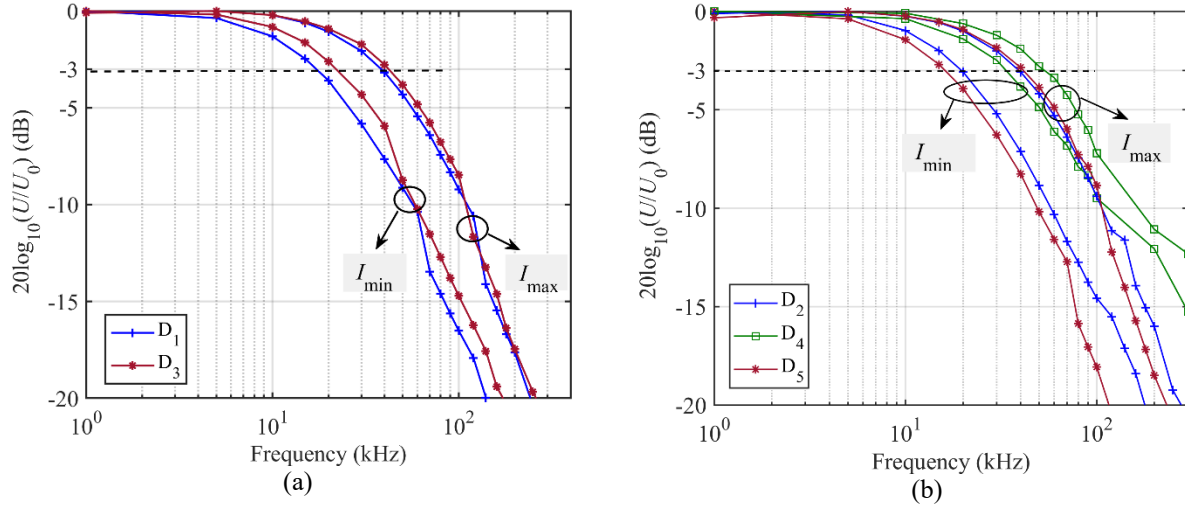
215 **Table 4** 3-term Gaussian model parameter for spatial intensity distribution for curvature with a radius of 11 and 8 cm

$k$	1	2	3
<b><math>r = 11</math> cm</b>			
$a_k$	0.9878	0.3054	0.2875
$b_k$	-0.7595	58.1	-59.42
$c_k$	51.59	32.99	31.94
<b><math>r = 8</math> cm</b>			
$a_k$	0.9814	0.3733	0.2721
$b_k$	4.832	-63.31	70.73
$c_k$	60.17	42.31	36.66

### 216 3.2.4 OLED bandwidth

217 To measure  $B_{\text{mod}}$  of the OLEDs, the devices were biased in the linear region of respective  $L-I$   
 218 curves, see Fig. 5. The measured frequency responses for D<sub>1</sub>-D<sub>5</sub> over a range of  $I_B$  are as shown  
 219 in Fig. 8, where  $U$  is the peak-to-peak received voltage and  $U_0$  is the peak-to-peak voltage of the  
 220 first sample. For comparison, the maximum and minimum bandwidth values as well as the  
 221 difference between them (i.e.,  $\Delta B$ ) are given in Table 5. The results for the devices tested show  
 222 that,  $B_{\text{mod}}$  increases with  $I_B$  as in agreement with (1). We also investigated the effect of bending  
 223 the flexible OLED on  $B_{\text{mod}}$  and observed no changes in  $B_{\text{mod}}$ . This is because the cut-off

224 frequency of OLED is defined by its physical parameters. This feature makes the OLED a  
 225 perfect optical antenna, where the same SNR is maintained over a given transmission radius.



226 **Fig. 8** The measured  $B_{\text{mod}}$  of: (a)  $D_{1, 3}$  and (b)  $D_{2, 4, 5}$ .

227 **Table 5** Bandwidth of OLEDs

Device	$B_{\text{mod-Min}}$ (kHz) ( $I_{B\text{-Min}}$ (mA))	$B_{\text{mod-Max}}$ (kHz) ( $I_{B\text{-Max}}$ (mA))	$\Delta B$ (kHz)
$D_1$	15 (40)	38 (250)	23
$D_2$	20 (100)	40 (600)	20
$D_3$	20 (100)	42 (280)	22
$D_4$	34 (30)	54 (60)	20
$D_5$	15 (40)	42 (250)	27

228

## 229 4 Experimental OVLC Link Results

### 230 4.1 Experimental test-bed for OVLC link with $m$ -CAP

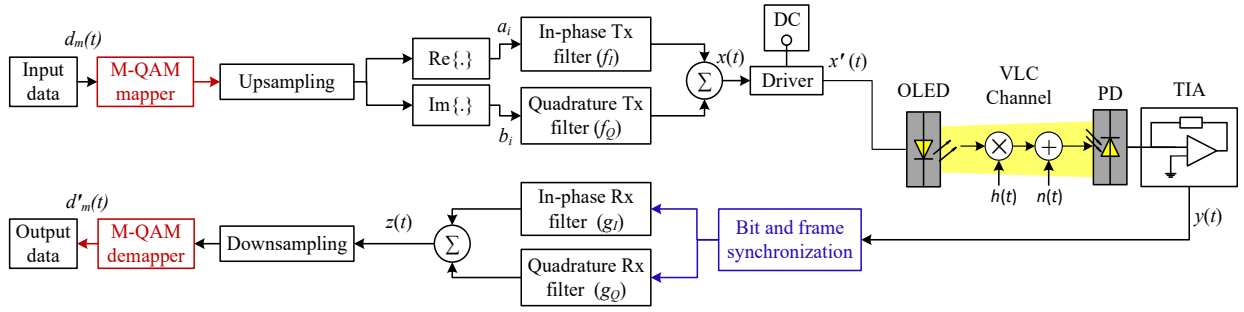
231 OLEDs with both high linearity and dynamic range can be used to support higher-order multi-  
 232 level and multi-carrier modulation schemes. However, in this work to simply demonstrate the  
 233 potential of the OLEDs as the transmitter in a VLC system, we have developed an experimental  
 234 test-bed to assess the link performance. We have adopted  $m$ -CAP modulation scheme due to (i)

235 reducing the effect of the highly bandlimited frequency response of OLEDs acting as a low-pass  
236 filter [42-44]; (ii) can be used as a multiuser scheme (e.g., personalized advertising) [45]; and  
237 (iii) implementation simplicity compared with the OFDM.

238 A block diagram of the experimental  $m$ -CAP OVLC link is shown in Fig. 9. Firstly,  $m$   
239 independent pseudo-random data streams  $d_m(t)$  of length 12,000 bits (memory depth limitation of  
240 the AFG) are generated and mapped onto the  $M$ -QAM (quadrature amplitude modulation)  
241 constellation where  $M$  is the order of the QAM. Note,  $M$  and  $m$  are selected as 16 and 2,  
242 respectively, in this work. During the experiment, a sufficient number of bits were transmitted to  
243 allow the measurement of the BER at  $10^{-6}$ . The linearity of OLEDs and their high dynamic range  
244 offer the potential to choose a number of carriers. Following upsampling, the real and the  
245 imaginary parts of the signal  $a_i$  and  $b_i$ , respectively, are applied to the in-phase and quadrature  
246 pulse shaping transmit filters, whose impulse responses form a Hilbert pair (i.e., they are  
247 orthogonal in the time domain). The transmit filters are formed as a product of the square root  
248 raised cosine (SRRC) filter pulse shapes and the sine and cosine waves for the quadrature and in-  
249 phase part of the signal, respectively. The carrier frequencies given by the transmit filters are set  
250 to 10 and 30 kHz for 1<sup>st</sup> and 2<sup>nd</sup> subcarriers ( $s_1$  and  $s_2$ ), respectively, in this work. The roll-off  
251 factor  $\beta$  used for the transmit pulse shapes is chosen as 0.15, given that the minimum bandwidth  
252 requirement is proportional to  $1 + \beta$ . Note, higher  $\beta$  leads to more protection against ISI for  
253 consistency with the literature [46]. The combined output from filters, i.e.,  $m$ -CAP signal  $x(t)$ , is  
254 applied to AFG and used via a driver for intensity modulation of the OLEDs. Following  
255 transmission over a short free space (up to 60 cm) line of sight (LoS) channel, the signal is  
256 detected using ORx Thorlabs PDA100A2. Subsequently, the output of ORx is captured using  
257 digital storage oscilloscope Keysight DSO9254A with the sampling frequency of 400 kS/s for

258 further off-line data processing. The regenerated electrical signal is given as  $y(t) = x'(t) \otimes h(t) +$   
 259  $n(t)$  where  $h(t)$  is the channel impulse response, the  $\otimes$  symbol denotes convolution, and the noise  
 260  $n(t)$  is mainly due to the ambient light and in the form of shot noise.  $y(t)$  is resampled to  
 261 transmitted signal by original sampling frequency prior to being applied to two time-reversed  
 262 filters  $g_I$  and  $g_Q$  matched to the transmit filters. The combined filter output  $z(t)$  followed down-  
 263 sampling are applied to the  $M$ -QAM demapper to re-generate the estimates transmitted data  
 264  $d'_m(t)$ . All the key system parameters are shown in Table 6.

265



266

267

**Fig. 9** The block diagram of the proposed OVLC system with  $m$ -CAP modulation.

268

**Table 6** The system parameters

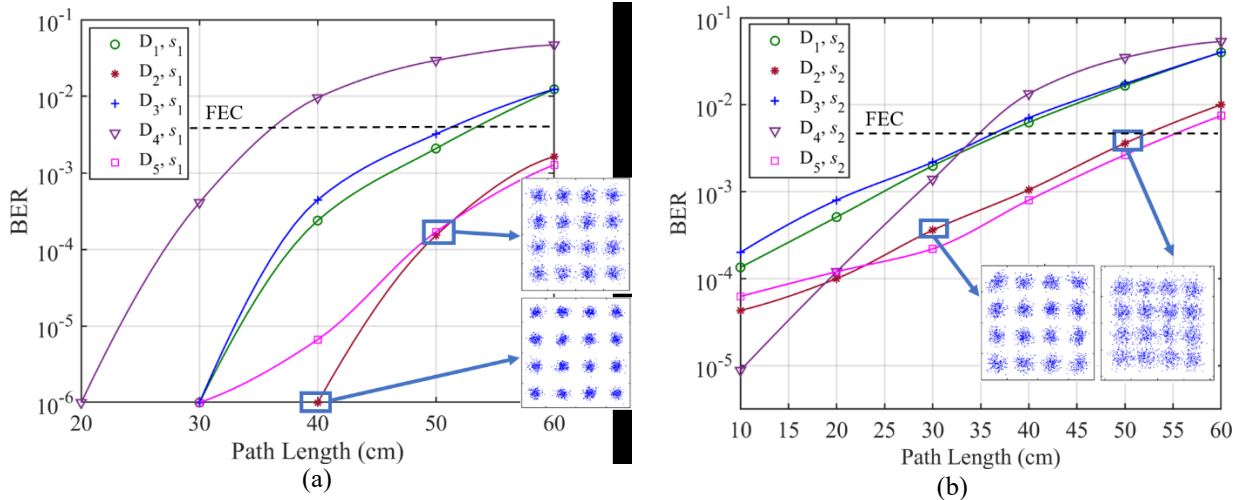
OLED	$I_B$ (mA)	$B_{mod}$ (kHz)	luminous flux (lm)	Area (cm <sup>2</sup> )
D <sub>1</sub>	160	28	58.5	74.5
D <sub>2</sub>	450	30	115.0	196.0
D <sub>3</sub>	160	32	52.0	100.0
D <sub>4</sub>	60	54	19.4	29.2
D <sub>5</sub>	180	34	68.4	100.0
ORx	Parameter	Value		
	Type of PD	Si-PIN		
	Active area of PD	75.4 mm <sup>2</sup>		
	Bandwidth	1.4 MHz at a 10 dB gain		
	Output voltage	0 to 10 V		
	Noise of amplifier	195 μV (RMS)		
	NEP	$6.75 \times 10^{-12}$ (W/√Hz) at $\lambda = 960$ nm		
	Responsivity	0.2 (A/W) at $\lambda = 400$ nm 0.5 (A/W) at $\lambda = 700$ nm		

269



270 4.2 Experimental results

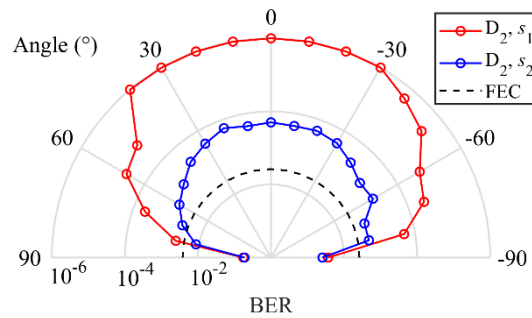
271 In this section, we evaluate the LoS OLED VLC link based on the BER for a range of  
 272 transmission span 10 to 60 cm and the OLED tilt angles  $\alpha$  from  $-90^\circ$  to  $90^\circ$ . The BER results  
 273 versus the path length for the OLED VLC and for  $s_1$  and  $s_2$  are shown in Figs. 10(a) and (b),  
 274 respectively along with the 7% forward error correction (FEC) BER limit of  $3.8 \times 10^{-3}$ . Examples  
 275 of measured constellation diagrams are shown as insets for  $D_2$  with two distance  $d$  of 40 and  
 276 50 cm and 30 and 50 cm for  $s_1$  and  $s_2$ , respectively. At the FEC BER limit, the transmission path  
 277 lengths for  $s_1$  are 36, 50, and  $\sim 60$  cm for  $D_4$ ,  $D_{1,3}$  and  $D_{2,5}$ , respectively, which are sufficient for  
 278 D2D communications. In the case of  $s_2$ , we observe a small decrease in the transmission spans by  
 279 2, 15, and 10 cm for  $D_4$ ,  $D_{1,3}$  and  $D_{2,5}$ , respectively compared with  $s_1$ . Although the path length  
 280 of 60 cm was obtained from our experiment, even longer distances can be achieved using OLED  
 281 panels made of materials with higher charge mobility giving higher  $B_{\text{mod}}$  [20, 47] or larger panels  
 282 with higher output optical power. To meet a given BER target and increase the transmission  
 283 span, the same SNR at a receiver and thus higher output optical power are required. Therefore,



284 **Fig. 10** The BER versus the path length for OLEDs with  $m$ -CAP for (a)  $s_1$  with the constellation diagrams for two distance of 40 and 50 cm for  $D_2$  and (b)  $s_2$  with the constellation diagrams for two distances of 30 and 50 cm for  $D_2$ .

285 organic devices with larger area (note decreased 3 dB bandwidth) or an array of OLEDs can be  
 286 utilized to follow these requirements. For instance, an OLED panel with a luminous flux of  
 287  $\sim 3000$  lm can support data transmission for distances up to 3 m.

288 For  $D_2$ , the BER plots in polar formats against  $\alpha$  are shown in Fig. 11 for  $s_1$  and  $s_2$ . Also  
 289 shown for comparison is the plot for the FEC BER limit. Note, the path length is fixed at 30 cm  
 290 (i.e., a BER  $< 10^{-6}$  when  $\alpha = 0^\circ$  see Fig. 10(a)). Note, the BER profiles display a symmetry about  
 291 the origin (i.e., the ORx is facing the OLED at  $\alpha$  of  $0^\circ$ ) offering improved performance over a  
 292 wide tilting angle. To meet the FEC limit,  $D_2$  can operate with  $\alpha$  up to  $\pm 80^\circ$  and  $\pm 70^\circ$  for  $s_1$  and  
 293  $s_2$ , respectively.



294  
 295 **Fig. 11** The polar plot of BER for tilted OLED ( $D_2$ ) with  $m$ -CAP for  $s_1$  and  $s_2$ .

## 296 5 Conclusions and Future Outlook

297 In this paper, we carried out characterization for a range of fixed and flexible OLEDs in  
 298 terms of their optical spectrum, power-current and illumination profiles. We showed that,  
 299 OLEDs offer stable illumination profile regardless of the bias current and a highly linear power-  
 300 current characteristic compared with the inorganic LEDs. We also showed that, the rigid OLEDs  
 301 beam pattern closely matches Lambertian with  $m_L = 1$ , whereas for curved OLED, the radiation  
 302 pattern displays a symmetry, which is wider than Lambertian as for curved OLED with a  
 303 curvature radius of 8 cm and a radiation angle of  $75^\circ$ . Based on the measured experimental data

304 for the curved OLED, we showed a new expression for the OLED's beam pattern, which follows  
305 the 3-term Gaussian profile with RMSE value of less than a standard error limit of 0.05 to assess  
306 the accuracy of the model. In addition, we evaluated OLED-based VLC systems for low data rate  
307 transmissions as in D2D communications. We showed the BER results of tilting OLED  
308 displayed a symmetry about the origin, with larger size OLEDs showing improved BER (i.e.,  
309 below the FEC limit) over a wider tilting angle (up to 80°, which is considerably large for D2D  
310 communications) and a longer transmission length (i.e., up to 60 cm).

### 311 *Acknowledgments*

312 This work is supported by the European Union's Horizon 2020 research and innovation  
313 programme under the Marie Skłodowska-Curie grant agreement no 764461 (VISION) and the  
314 Czech Rep. funded project GACR 17-17538S.

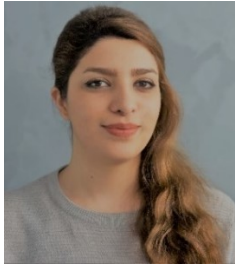
### 315 *References*

- 316 [1] Z. Ghassemlooy, L. N. Alves, S. Zvanovec, and M.-A. Khalighi, *Visible Light Communications: Theory and Applications*. CRC Press, 2017.
- 317 [2] Z. Ghassemlooy, W. Popoola, and S. Rajbhandari, *Optical wireless communications: system and channel modelling with Matlab®*, 2nd ed. CRC press, 2019.
- 318 [3] P. H. Pathak, X. Feng, P. Hu, and P. Mohapatra, "Visible light communication, networking, and sensing: A survey, potential and challenges," *IEEE communications surveys & tutorials*, vol. 17, no. 4, pp. 2047-2077, 2015.
- 319 [4] P. A. Haigh *et al.*, "Organic visible light communications: Recent progress," in *2014 16th International Conference on Transparent Optical Networks (ICTON)*, 2014: IEEE, pp. 1-5.
- 320 [5] P. Binh and N. Hung, "High-speed visible light communications using ZnSe-based white light emitting diode," *IEEE Photonics Technology Letters*, vol. 28, no. 18, pp. 1948-1951, 2016.
- 321 [6] J. Yang *et al.*, "Highly uniform white light-based visible light communication using red, green, and blue laser diodes," *IEEE Photonics Journal*, vol. 10, no. 2, pp. 1-8, 2018.
- 322 [7] T.-C. Wu, Y.-C. Chi, H.-Y. Wang, C.-T. Tsai, Y.-F. Huang, and G.-R. Lin, "Tricolor R/G/B laser diode based eye-safe white lighting communication beyond 8 Gbit/s," *Scientific reports*, vol. 7, no. 1, p. 11, 2017.
- 323 [8] P. A. Haigh, Z. Ghassemlooy, S. Rajbhandari, and I. Papanikolaou, "Visible light communications using organic light emitting diodes," *IEEE Communications Magazine*, vol. 51, no. 8, pp. 148-154, 2013.
- 324 [9] P. Haigh, "Using equalizers to increase data rates in organic photonic devices for visible light communications systems," University of Northumbria, 2014.

- 337 [10] J. Ràfols-Ribé *et al.*, "High-performance organic light-emitting diodes comprising ultrastable  
338 glass layers," *Science advances*, vol. 4, no. 5, p. eaar8332, 2018.
- 339 [11] J. Clark and G. Lanzani, "Organic photonics for communications," *Nature photonics*, vol. 4, no.  
340 7, p. 438, 2010.
- 341 [12] P. Luo, M. Zhang, Z. Ghassemlooy, S. Zvanovec, S. Feng, and P. Zhang, "Undersampled-based  
342 modulation schemes for optical camera communications," *IEEE Communications Magazine*, vol.  
343 56, no. 2, pp. 204-212, 2018.
- 344 [13] Y. Li, Z. Ghassemlooy, X. Tang, B. Lin, and Y. Zhang, "A VLC smartphone camera based  
345 indoor positioning system," *IEEE Photonics Technology Letters*, vol. 30, no. 13, pp. 1171-1174,  
346 2018.
- 347 [14] R. Boubezari, H. Le Minh, Z. Ghassemlooy, and A. Bouridane, "Smartphone camera based  
348 visible light communication," *Journal of Lightwave Technology*, vol. 34, no. 17, pp. 4121-4127,  
349 2016.
- 350 [15] B. Lin, Z. Ghassemlooy, C. Lin, X. Tang, Y. Li, and S. Zhang, "An indoor visible light  
351 positioning system based on optical camera communications," *IEEE Photonics Technology  
352 Letters*, vol. 29, no. 7, pp. 579-582, 2017.
- 353 [16] Q. Wang *et al.*, "Light positioning: A high-accuracy visible light indoor positioning system based  
354 on attitude identification and propagation model," *International Journal of Distributed Sensor  
355 Networks*, vol. 14, no. 2, p. 1550147718758263, 2018.
- 356 [17] J. H. Burroughes *et al.*, "Light-emitting diodes based on conjugated polymers," *nature*, vol. 347,  
357 no. 6293, p. 539, 1990.
- 358 [18] C. W. Tang and S. A. VanSlyke, "Organic electroluminescent diodes," *Applied physics letters*,  
359 vol. 51, no. 12, pp. 913-915, 1987.
- 360 [19] Z. H. Kafafi, *Organic electroluminescence*. CRC Press, 2018.
- 361 [20] W. Zhu *et al.*, "Graphene radio frequency devices on flexible substrate," *Applied Physics Letters*,  
362 vol. 102, no. 23, p. 233102, 2013.
- 363 [21] P. A. Haigh *et al.*, "A 20-Mb/s VLC link with a polymer LED and a multilayer perceptron  
364 equalizer," *IEEE Photonics Technology Letters*, vol. 26, no. 19, pp. 1975-1978, 2014.
- 365 [22] H. Chen, Z. Xu, Q. Gao, and S. Li, "A 51.6 Mb/s Experimental VLC System Using a  
366 Monochromic Organic LED," *IEEE Photonics Journal*, vol. 10, no. 2, pp. 1-12, 2017.
- 367 [23] T. Yamada, "Latest Development of Soluble-OLED Material and its Application to Mid-to large-  
368 sized Panel Production," in *2019 26th International Workshop on Active-Matrix Flatpanel  
369 Displays and Devices (AM-FPD)*, 2019, vol. 26: IEEE, pp. 1-4.
- 370 [24] H. J. Shin and T. W. Kim, "Ultra-High-Image-Density, Large-Size Organic Light-Emitting  
371 Device Panels Based on Highly Reliable Gate Driver Circuits Integrated by Using InGaZnO  
372 Thin-Film Transistors," *IEEE Journal of the Electron Devices Society*, vol. 7, pp. 1109-1113,  
373 2019.
- 374 [25] J. Smith *et al.*, "Application of flexible flat panel display technology to wearable biomedical  
375 devices," *Electronics Letters*, vol. 51, no. 17, pp. 1312-1314, 2015.
- 376 [26] T. Kasahara, H. Kuwae, and J. Mizuno, "New Era of Device Science," in *2019 Pan Pacific  
377 Microelectronics Symposium (Pan Pacific)*, 2019: IEEE, pp. 1-6.
- 378 [27] J. Kalinowski, *Organic Light-Emitting Diodes: Principles, Characteristics & Processes*. CRC  
379 press, 2018.
- 380 [28] P. Deng, M. Kavehrad, and M. A. Kashani, "Nonlinear modulation characteristics of white LEDs  
381 in visible light communications," in *Optical Fiber Communication Conference*, 2015: Optical  
382 Society of America, p. W2A. 64.
- 383 [29] P. A. Haigh *et al.*, "Wavelength-multiplexed polymer LEDs: Towards 55 Mb/s organic visible  
384 light communications," *IEEE Journal on Selected Areas in Communications*, vol. 33, no. 9, pp.  
385 1819-1828, 2015.

- 386 [30] S. T. Le *et al.*, "10 Mb/s visible light transmission system using a polymer light-emitting diode  
387 with orthogonal frequency division multiplexing," *Optics letters*, vol. 39, no. 13, pp. 3876-3879,  
388 2014.
- 389 [31] A. Burton *et al.*, "Optoelectronic Modelling, Circuit Design and Modulation for Polymer-Light  
390 Emitting Diodes for Visible Light Communication Systems," in *2019 26th International  
391 Conference on Telecommunications (ICT)*, 2019: IEEE, pp. 55-59.
- 392 [32] A. Burton, H. Le Minh, Z. Ghassemlooy, S. Rajbhandari, and P. A. Haigh, "Smart receiver for  
393 visible light communications: Design and analysis," in *2012 8th International Symposium on  
394 Communication Systems, Networks & Digital Signal Processing (CSNDSP)*, 2012: IEEE, pp. 1-5.
- 395 [33] Z. Zeng, M. D. Soltani, M. Safari, and H. Haas, "Angle Diversity Receiver in LiFi Cellular  
396 Networks," in *ICC 2019-2019 IEEE International Conference on Communications (ICC)*, 2019:  
397 IEEE, pp. 1-6.
- 398 [34] C. Chen, M. D. Soltani, M. Safari, A. A. Purwita, X. Wu, and H. Haas, "An omnidirectional user  
399 equipment configuration to support mobility in LiFi networks," in *2019 IEEE International  
400 Conference on Communications Workshops (ICC Workshops)*, 2019: IEEE, pp. 1-6.
- 401 [35] M. D. Soltani *et al.*, "Bidirectional Optical Spatial Modulation for Mobile Users: Toward a  
402 Practical Design for LiFi Systems," *IEEE Journal on Selected Areas in Communications*, vol. 37,  
403 no. 9, pp. 2069-2086, 2019.
- 404 [36] N. V. Khanh, P. Q. Thai, N. H. Duy, and N. N. A. Khoa, "Investigation on MIMO OLED VLC  
405 System Performance," in *Novel Optical Materials and Applications*, 2018: Optical Society of  
406 America, p. JTU5A. 61.
- 407 [37] P. A. Haigh *et al.*, "A MIMO-ANN system for increasing data rates in organic visible light  
408 communications systems," in *2013 IEEE International Conference on Communications (ICC)*,  
409 2013: IEEE, pp. 5322-5327.
- 410 [38] H. Chen *et al.*, "A 1.9 Mbps OFDM-based all-organic visible light communication system," in  
411 *2016 IEEE International Conference on Communication Systems (ICCS)*, 2016: IEEE, pp. 1-6.
- 412 [39] P. Haigh *et al.*, "Organic visible light communications: Methods to achieve 10 Mb/s," in *2017  
413 IEEE Photonics Conference (IPC)*, 2017: IEEE, pp. 553-554.
- 414 [40] M. Dyble, N. Narendran, A. Bierman, and T. Klein, "Impact of dimming white LEDs:  
415 Chromaticity shifts due to different dimming methods," in *Fifth international conference on solid  
416 state lighting*, 2005, vol. 5941: International Society for Optics and Photonics, p. 5941 1H.
- 417 [41] J. W. Gorman and R. Toman, "Selection of variables for fitting equations to data,"  
418 *Technometrics*, vol. 8, no. 1, pp. 27-51, 1966.
- 419 [42] P. A. Haigh *et al.*, "Multi-band carrier-less amplitude and phase modulation for bandlimited  
420 visible light communications systems," *IEEE Wireless Communications*, vol. 22, no. 2, pp. 46-53,  
421 2015.
- 422 [43] P. A. Haigh *et al.*, "A multi-CAP visible-light communications system with 4.85-b/s/Hz spectral  
423 efficiency," *IEEE Journal on Selected Areas in Communications*, vol. 33, no. 9, pp. 1771-1779,  
424 2015.
- 425 [44] P. Chvojka *et al.*, "On the m-CAP performance with different pulse shaping filters parameters for  
426 visible light communications," *IEEE Photonics Journal*, vol. 9, no. 5, pp. 1-12, 2017.
- 427 [45] M. M. Merah, H. Guan, and L. Chassagne, "Experimental Multi-User Visible Light  
428 Communication Attocell Using Multiband Carrierless Amplitude and Phase Modulation," *IEEE  
429 Access*, vol. 7, pp. 12742-12754, 2019.
- 430 [46] M. I. Olmedo *et al.*, "Multiband carrierless amplitude phase modulation for high capacity optical  
431 data links," *Journal of Lightwave Technology*, vol. 32, no. 4, pp. 798-804, 2013.
- 432 [47] K. Yoshida *et al.*, "245 MHz bandwidth organic light-emitting diodes used in a gigabit optical  
433 wireless data link," *Nature Communications*, vol. 11, no. 1, pp. 1-7, 2020.
- 434

435 *Biographies*



**Zahra Nazari Chaleshtori** received her MSc degree in 2016 from Isfahan University of Technology, Iran. Now, she is a PhD candidate at Czech Technical University (CTU) in Prague, Czech Republic. She is focused on the utilization of organic LED-based visible light communications for device-to-device. She is involved in EU H2020 Marie Skłodowska-Curie Innovative Training Network (VisIoN 764461) and also a member of Wireless and Fiber Optics team at CTU.

436



**Andrew Burton** received the BEng (Hons.), MSc degrees (distinction) and PhD from Northumbria University, UK. Since graduation he worked as Research Fellow at Northumbria University until 2019, when he joined ISOCOM company as a Technical Manager. His research interests include electronics, optical communications and visible-light communications.

437



**Prof. Stanislav Zvanovec** received the M.Sc. and Ph.D. degrees from the Czech Technical University (CTU) in Prague, in 2002 and 2006, respectively. He is a Full Professor, the Deputy Head of the Department of Electromagnetic Field and leader of Wireless and Fiber Optics team at CTU. His current research interests include FSO and fiber optical systems, VLC, RF over optics. He is author of two books and more than 250 journal articles and conference papers.

438



**Prof. Zabih Ghassemlooy FOSA, FIET, SMIEEE:** BSc(Hons.) EE Engineering, Manchester Metropolitan Univ., (1981), MSc (1984) and PhD (1987), Manchester Univ., UK. 1987-88 Post-Doctoral Research Fellow, City Univ., UK. 2004-14 Associate Dean Research, Faculty of Eng. & Env., Northumbria Univ. Head of Optical Communications Research Group. Research Fellow(2016) and Distinguished Professor(2015), Chinese Academy of Science. 850 publications. Research: optical wireless communications, free space optics, visible light communications. Chief Editor: British J. of Applied Science and Technology.

439



**Petr Chvojka** received M.Sc. and Ph.D. degrees from the Faculty of Electrical Engineering, Czech Technical University (CTU) in Prague, in 2013 and 2018, respectively. He currently works as a Research Fellow at the Department of Electromagnetic Field, CTU in Prague, where he is a member of the Wireless and Fiber Optics Group. His research focuses on optical systems design and modelling, including inorganic and organic devices and digital signal processing techniques for visible light communications.

440